

1 **Use of a global model to understand speciated atmospheric mercury observations at five high-elevation sites**

2  
3  
4  
5  
6  
7  
8  
9  
10  
11  
12  
13  
14  
15  
16  
17  
18  
19  
20  
21

Peter Weiss-Penzias<sup>1</sup>, Helen M. Amos<sup>2</sup>, Noelle E. Selin<sup>3</sup>, Mae Sexauer Gustin<sup>4</sup>, Daniel A. Jaffe<sup>5</sup>, Daniel Obrist<sup>6</sup>, Guey-Rong Sheu<sup>7</sup>, Amanda Giang<sup>3</sup>

<sup>1</sup>University of California, Santa Cruz

<sup>2</sup>Harvard University

<sup>3</sup>Massachusetts Institute of Technology

<sup>4</sup>Department of Natural Resources and Environmental Science, University of Nevada, Reno

<sup>5</sup>University of Washington, Bothell

<sup>6</sup>Desert Research Institute

<sup>7</sup>National Central University, Taiwan

Keywords: gaseous oxidized mercury (GOM), free troposphere, GEOS-Chem, ozone, photochemistry

## Abstract

Atmospheric mercury (Hg) measurements using the Tekran<sup>®</sup> analytical system from 5 high-elevation sites (1400-3200 m elevation), one in Asia and 4 in the western U.S., were compiled over multiple seasons and years, and these data were compared with the global model GEOS-Chem. Mercury data consisted of gaseous elemental Hg (GEM) and “reactive Hg” (RM) which is a combination of the gaseous oxidized (GOM) and particulate bound (<2.5 μm) (PBM) fractions as measured by the Tekran<sup>®</sup> system. We used a subset of the observations by defining a “free tropospheric” (FT) dataset by screening using measured water vapor mixing ratios. The oxidation scheme used by the GEOS-Chem model was varied between the standard run with Br oxidation and an alternative run with OH-O<sub>3</sub> oxidation. We used this model-measurement comparison to help interpret the spatio-temporal trends in, and relationships among the Hg species and ancillary parameters to better understand the sources and fate of atmospheric RM. The most salient feature of the data across sites, seen more in the summer relative to the spring, was that RM was negatively correlated with GEM and water vapor mixing ratios (WV) and positively correlated with ozone (O<sub>3</sub>) both in the standard model and the observations, indicating that RM was formed in dry upper altitude air from the photo-oxidation of GEM. During a free tropospheric transport high RM event observed sequentially at 3 sites from Oregon to Nevada, the slope of the RM/GEM relationship at the westernmost site was  $-1020 \pm 209 \text{ pg ng}^{-1}$ , indicating near quantitative GEM to RM photochemical conversion. An improved correlation between the observations and the model was seen when the model was run with the OH-O<sub>3</sub> oxidation scheme instead of the Br oxidation scheme. This simulation produced higher concentrations of RM and lower concentrations of GEM, especially at the desert sites in northwestern Nevada. This suggests that future work should investigate the effect of Br- and O<sub>3</sub>- initiated gas-phase oxidation occurring simultaneously in the atmosphere, as well as aqueous and heterogeneous reactions to understand if there are multiple global oxidants for GEM and hence multiple forms of RM in the atmosphere. If the chemical forms of RM were known, then the collection efficiency of the analytical method could be better evaluated.

## 1.0 Introduction

Mercury (Hg) is a neurotoxin that persists in the environment and bioaccumulates in food chains. It is dispersed globally by long-range atmospheric transport (Schroeder and Munthe, 1998; Strode et al., 2008). Anthropogenic sources emit Hg to the atmosphere as gaseous elemental mercury (GEM) and divalent chemical compounds (Hg<sup>II</sup>), whereas natural sources are thought to emit predominantly GEM (Pirrone et al., 2010). Oxidized atmospheric compounds (also termed Reactive Mercury = RM = Gaseous Oxidized Mercury (GOM) + Particulate Bound Mercury (PBM)) are typically measured as two operationally-defined forms. The first is adsorbed onto a KCl (potassium chloride)-coated denuder and latter collected on quartz-fiber filters (Landis et al., 2002). Gaseous oxidized Hg is water soluble and removed rapidly from the atmosphere in wet deposition (Lindberg and Straton, 1998), however it may be transported long distances in the free troposphere (Huang et al., 2012; Ambrose et al., 2012, Wright et al., 2013). Dry deposition is also thought to be an important sink for GOM and this has been demonstrated using surrogate surfaces. (cf. Gustin et al, 2012; Wright et al,

2013; Huang et al., 2013, Sather et al., 2013, Castro et al., 2013). The lifetime of PBM, limited by particle size, is typically less than 10 days (Schroeder and Munthe, 1998). Gaseous elemental Hg has lower water solubility and an atmospheric lifetime on the order of months to a year (Schroeder and Munthe, 1998). This form may also make a contribution to dry deposition of equivalent magnitude to GOM (Zhang et al., 2012). Gaseous elemental Hg atoms may be re-emitted depending on the surfaces on which they land (Gustin, 2011).

Most measurements of Hg forms made using the Tekran® system have found that GEM comprises 95-100% of total Hg (Valente et al., 2007), a result of the long lifetime of GEM, and the rapid removal of GOM and PBM by wet and dry deposition. However, observations in the free troposphere (FT) from a mountain-top site have shown that the concentrations of GOM can be roughly equivalent to the concentrations of GEM during brief periods (Swartzendruber et al., 2006; Timonen et al., 2013). Observations from aircraft have shown depletion of GEM in the upper troposphere/lower stratosphere (Talbot et al., 2007; Swartzendruber et al., 2008; Lyman and Jaffe, 2011), consistent with a previous hypothesis that Hg is contained within particles in this region of the atmosphere (Murphy et al., 2006). Recent measurements of oxidized forms from aircraft at an altitude of near 6 km have shown a strong correlation with ozone and potential vorticity, both tracers of stratospheric air (Lyman and Jaffe, 2011). It is currently thought the process of formation of GOM in the upper atmosphere involves the oxidation of GEM by Br atoms (formed from BrO) (Holmes et al., 2006) but there is no current consensus (Subir et al., 2011). Early experiments with Hg+O<sub>3</sub> (Hall, 1995) were likely influenced by wall effects (Hynes et al., 2009) and theoretical calculations from Goodsite et al. (2004) suggest the Hg+OH reaction is not likely in the atmosphere. However, Dibble et al. (2013) suggested that a HgBr+OH reaction is possible.

There is a current discussion among the atmospheric mercury measurement community that the Tekran® analytical system may produce GOM and PBM measurements that are biased too low due to poor uptake efficiency of the KCl-denuder and quartz filter, and interferences due to the presence of ozone (O<sub>3</sub>) (Gustin and Jaffe, 2010; Gustin et al., 2013; Ambrose et al., 2013; Huang et al., 2013; Kos et al., 2013; Huang et al., 2014; Jaffe et al. 2014; McClure et al., 2014). On the other hand, some studies have seen quantitative conversion of GEM to RM during events, as well as zero GEM concentrations coinciding with large RM concentrations (Moore et al., 2013; 2014) suggesting that the analytical system may perform more accurately in some environments with extreme low humidity. Thus, a goal of this study was to compare available Tekran® instrument measurements of GEM/GOM/PBM along with ozone and meteorology from five surface sites that have reported interception of dry free troposphere air, with simulated speciated Hg concentrations from the GEOS-Chem Hg coupled atmosphere-ocean-land model (Amos et al., 2012) in order to examine spatio-temporal trends both in the observations and the model. Reactive Hg (RM = GOM+PBM) was used throughout this paper because given the uncertainty and the GOM/PBM equilibria, RM is a more meaningful quantity than the individual species. This is the first attempt to compare observations across high elevation sites and incorporate model data to constrain the processes important for RM. In addition, we examined OH+O<sub>3</sub> chemistry in the model as an

89 alternative to the standard model run that uses Br as the oxidant, and compared with the observations to reveal any  
90 clues about the likely oxidation mechanism for GEM.

## 92 **2.0 Methods**

### 93 *2.1 Site Characteristics*

94 Maps depicting the locations of the study sites are shown in Figure SI-1. Site characteristics and the date ranges  
95 of the model-observation comparisons are given in Table 1. Four sites in this study are located in the temperate  
96 latitudes of North America, in the intermountain west. Two of these sites are on mountain-tops: Mount Bachelor  
97 Observatory (MBO) and Storm Peak Laboratory (SPL). Two other sites are within the Basin and Range province of  
98 Nevada: Desert Research Institute near Reno (DRI) and Paradise Valley north of Winnemucca (NV02). The fifth site, Lulin  
99 Atmospheric Background Station (LABS) is a tropical mountaintop location on the island of Taiwan in East Asia. Details  
100 of all these sites have been discussed elsewhere (Sheu et al., 2010, Swartzendruber et al., 2008, Stamenkovic et al.,  
101 2008, Weiss-Penzias et al., 2009, Fain et al., 2009). The LABS site observed polluted air due to Asian outflow primarily in  
102 spring, fall and winter (Sheu et al., 2010) and biomass burning emissions from the Indochina Peninsula in the spring  
103 (Sheu et al., 2012). Likewise, Asian long-range transport of GEM has been observed at MBO and SPL in the spring (Jaffe  
104 et al., 2005; Obrist et al., 2008). The DRI and NV02 sites were operated by University of Nevada, Reno from 2005 to  
105 2007 (Peterson et al. 2009) and during the summer of 2007 (Lyman and Gustin, 2008), respectively. All sites have  
106 reported enhanced concentrations of GOM during periods of dry air and low GEM.

### 108 *2.2 Speciated Hg and Ancillary Measurements*

109 At all sites GEM, GOM, and PBM were measured with the Tekran® 2537/1130/1135 automated CVAFS  
110 instrument. Details of the Hg measurements, along with O<sub>3</sub> and meteorology are described in detail elsewhere  
111 (Swartzendruber et al., 2006, Fain et al., 2009; Peterson et al., 2009; Lyman and Gustin, 2008; Sheu et al., 2010). Briefly,  
112 air is drawn into an inlet with a 2.5 μm size cut impactor into a KCl-coated denuder which absorbs GOM (unknown  
113 efficiency), then through a quartz fiber filter which is hypothesized to collect PBM, and finally across alternating Au  
114 cartridges which adsorb GEM. Gaseous elemental Hg measurements are recorded every 5-min, while GOM and PBM are  
115 collected for 2 hours and desorbed for 1 hour, giving a measurement every 3-hours. Concentration units are ng m<sup>-3</sup> at  
116 STP (273.14 K and 1 atm) for GEM and pg m<sup>-3</sup> at STP for GOM and PBM.

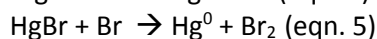
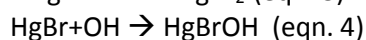
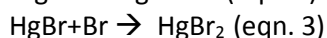
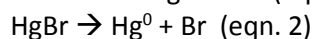
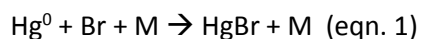
117 The uncertainty in the GEM measurement when compared with other instruments is typically < 10% (Lyman et  
118 al., 2007). While the RAMIX results for GEM did identify one out of 4 instruments that had a significant discrepancy, 3  
119 out of the 4 instruments had very similar response for GEM (within 10%) (Gustin et al 2013). Another recent  
120 intercomparison also determined the average systematic uncertainty for Tekran® GEM measurements to be < 10%, but  
121 in some extreme cases can be up to 20% (Slemr et al., 2014). Thus, while the instruments in this study were not

122 compared side-by-side, they were operated by trained technicians and likely produced results with the normal range of  
123 uncertainty.

124 GEM can be calibrated with a primary source, but currently there is no calibrant for GOM or PBM, a serious  
125 limitation to the accuracy of the GOM and PBM data (Gustin and Jaffe, 2010; Jaffe et al., 2014). Furthermore, ambient  
126 ozone concentrations negatively interfere with the adsorption and retention of GOM on the denuder (Lyman et al.,  
127 2010). There is also recent evidence that GOM may be composed of various forms of Hg, including HgCl<sub>2</sub>, HgBr<sub>2</sub>, etc.,  
128 and that the KCl-coated denuder may not collect all these forms with equivalent efficiency (Gustin et al., 2012, Huang et  
129 al., 2013, Gustin et al., 2013). In addition to the denuder, some fraction of GOM may be collected on the quartz fiber  
130 filter in the particulate Hg instrument (Tekran®-1135) (Gustin et al., 2013), and for these reasons we present GOM +  
131 PBM = reactive Hg (RM) measurements in this paper. A recent inter-comparison between Tekran® and new Hg  
132 measurement methods was performed and it was found that the Tekran® RM measurements were systematically 2-3  
133 times lower than Hg<sup>II</sup> measured with other methods (Gustin et al., 2013; Huang et al., 2013). Thus, the Tekran®  
134 measurements reported in this paper, while representing the best available observations, must be treated with caution  
135 in light of these uncertainties, and are likely a lower bound to the actual concentrations of RM. However, despite these  
136 uncertainties, we hypothesized comparing speciated Hg data from these high-elevation sites would be useful for  
137 comparing site-to-site variability and RM/GEM slopes.

### 138 2.3 GEOS-Chem Model

139 Model output was from version 9-01-01 of the GEOS-Chem (GC) Hg coupled atmosphere-ocean-land model  
140 (www.geos-chem.org), described in detail elsewhere (Amos et al., 2012). Briefly, the simulation was conducted for  
141 2004-2009 with GEOS-5 assimilated meteorological and surface data from the NASA Global Modeling and Assimilation  
142 Office (GMAO) at the 2° x 2.5° resolution. The GEOS-Chem simulation transports 2 Hg tracers in the atmosphere: Hg<sup>0</sup>  
143 and Hg<sup>II</sup>. The concentration units, as with the observations, are ng m<sup>-3</sup> at STP (273.14 K and 1 atm) for GEM and pg m<sup>-3</sup>  
144 at STP for GOM and PBM. We will compare results from a simulation with Br chemistry versus one with OH and ozone  
145 chemistry. While both oxidation mechanisms, and possibly others, may operate together in the real atmosphere, these  
146 idealized simulations enable us to explore the constraints that observations place on the atmospheric chemistry of  
147 mercury. Mercury redox chemistry in the standard GC model followed Holmes et al. (2010), with oxidation of Hg<sup>0</sup> by Br  
148 atoms according to the following reactions:



155 For rate expressions of these reactions see Holmes et al. (2010). Photoreduction of Hg<sup>II</sup> occurs in liquid cloud droplets.  
156 Alternatively, oxidation of Hg<sup>0</sup> can proceed via OH and O<sub>3</sub> in GEOS-Chem according to the following reactions (Pal and  
157 Ariya, 2004; Hall, 1995; Sommar et al., 2001; Selin et al., 2007):



161 Anthropogenic emissions are from GEIA 2005 inventory (Pacyna et al., 2010). Model output is taken from pressure  
162 levels consistent with each site, and mean modeled values, on seasonal, daily, 12-hour, and 3-hour timescales, were  
163 compared with observations. Ancillary model output data (O<sub>3</sub>, Water Vapor (WV), and Temperature (T)) were generated  
164 from the v9-01-01 full chemistry simulation. GEOS-Chem has been extensively evaluated against Mercury Deposition  
165 Network wet deposition observations (Amos et al., 2012; Holmes et al., 2010; Selin and Jacob, 2008) as well as surface  
166 land-based sites, ship cruises, and plane flight data of GEM and seawater concentrations (Selin et al., 2008; Holmes et al.  
167 2010; Soerensen et al., 2010; Amos et al., 2012).

168

#### 169 *2.4 FT Subset of Data Based on Water Vapor Measurements*

170 The global chemical transport model used here cannot resolve local effects that sometimes influenced the  
171 measurements at each site. The model is sampling in the free troposphere (FT) but each site had time periods where  
172 the air was from the boundary layer (BL) influenced by surface Hg sources and sinks. Comparisons between the  
173 observations and the model were made applying a WV cutoff of WV < 75<sup>th</sup> percentile based on seasonal data sets (Table  
174 SI-1). The drier air data set was termed “FT” and was used for model comparisons. The seasonal months were: March-  
175 May = spring, June-August = summer, September-November = fall, and December-February = winter. This cutoff was  
176 evaluated by examining NO+NO<sub>2</sub>=NO<sub>x</sub> concentrations at one site in Nevada (NV02) during the summer of 2007, where it  
177 was found that when WV < 75<sup>th</sup> percentile, mean NO<sub>x</sub> was 0.12 ppb and when WV was in the upper 25<sup>th</sup> percentile,  
178 mean NO<sub>x</sub> = 0.53 ppb. This supported our use of the cutoff. The drier air contained less NO<sub>x</sub>, and thus less influence from  
179 the BL. At NV02, NO<sub>x</sub> was positively correlated with GEM (r<sup>2</sup> = 0.57) and thus applying the WV screen to these data also  
180 removed very high GEM concentrations (> 6 ng m<sup>-3</sup>), likely from geogenic sources at the surface, from the FT data set.  
181 Applying a more stringent WV cutoff, such as < 50<sup>th</sup> percentile, would select data with even less influence from the BL,  
182 but would have less statistical power due to small numbers of observations. Thus, the 75<sup>th</sup> percentile WV cutoff was  
183 chosen for all sites. Water vapor screens have been used previously based on the empirically-derived equations  
184 described in Bolton (1980):

$$185 \quad WV(gkg^{-1}) = [RH * (6.22) \frac{0.01 * e^{(77.345 + 0.0057T_{amb} - \frac{7235}{T_{amb}})}}{T_{amb}^{8.2}}] (P^{-1}) \text{ (eqn. 10)}$$

186 where RH is relative humidity, T<sub>amb</sub> is the ambient temperature in Kelvin, and P is the barometric pressure in hPa (Weiss-  
187 Penzias et al., 2006; 2009, Ambrose et al., 2011; Faïn et al., 2009; Sheu et al., 2010). Since barometric pressure data

188 were not available for each site, a constant P was assumed for each site, based on the elevation of each site, which adds  
189 < 1% error to the WV calculation.

## 191 2.4 Statistical Analyses

192 Statistical calculations were performed with Origin 9.1. Comparisons between population means were  
193 considered significantly different based on a paired t-test or ANOVA with  $p < 0.05$ . For correlations between species in  
194 the observations and the model daily means were used to avoid biases associated with diel variations. The model  
195 output and the observations were compared over equivalent time periods on the same time resolution.

## 197 3.0 Results and Discussion

### 198 3.1 Spatial and Temporal Trends in the Observations

199 Mean measured GEM concentration was highest at LABS during the spring ( $2.2 \text{ ng m}^{-3}$ ) likely due to Asian  
200 outflow impacting the island of Taiwan during this season (Sheu et al., 2010) (Figure 1). The lowest observed seasonal  
201 mean GEM concentration occurred at DRI during the summer at  $1.36 \text{ ng m}^{-3}$ , simultaneous with the highest observed  
202 RM measurements suggesting photochemical conversion of GEM (Weiss-Penzias et al., 2009). Summertime GEM was  
203 lower compared to all other seasons at the sites with measurements in multiple seasons (MBO, DRI, LABS, SPL). Mean  
204 GEM concentrations from the unfiltered data set were larger than from the FT data set at NV02 (summer) and DRI  
205 (summer), but the opposite trend was observed at MBO (spring) and LABS (spring). This suggests the desert sites were  
206 influenced more by local surface sources (Lyman and Gustin, 2008) whereas MBO and LABS have observed springtime  
207 Asian long-range transport of GEM in the FT (Jaffe et al., 2005; Sheu et al., 2010).

208 Measured RM concentrations varied by a about a factor of 7 between sites, with the highest concentrations  
209 occurring during summertime dry air conditions at DRI, MBO and SPL (Figure 1). At the tropical site (LABS), summertime  
210 RM was at its seasonal minimum due to high humidity and rapid loss from wet deposition, but during the spring RM was  
211 enhanced when the conditions at LABS were drier and more conducive to long-range transport. The FT data showed  
212 higher mean RM at every site and season with notable increases of 40%, 20%, and 15% for MBO summer, SPL summer,  
213 and DRI summer compared to unfiltered RM mean concentrations. This suggests that air from the FT at these sites was  
214 generally enhanced in RM and depleted in GEM, reflecting the photochemical loss of GEM and longer lifetime of RM in  
215 the FT.

216 Measured  $\text{O}_3$  concentrations were 15-20% higher during the spring compared to the summer at the North  
217 American mountain top sites (MBO, SPL), which is different from the RM seasonal maximum in summer (Table SI-1). The  
218 desert sites located in Nevada showed WV mixing ratios equivalent to, or below those at the mountaintop sites during  
219 the summer.

### 220 3.2 Standard Model-Measurement Comparison

221 The standard model showed the highest mean GEM concentration among all sites at LABS ( $2.10 \text{ ng m}^{-3}$ ) during  
222 the spring (Figure 1), which was in close agreement with the observations ( $2.20 \text{ ng m}^{-3}$ ) (Table SI-1). At all sites, the  
223 direction of the seasonal trend in GEM in the standard model agreed with the observations (spring > summer). The best  
224 agreement was at MBO where spring mean GEM concentrations were 11% greater than summer GEM concentrations in  
225 both the standard model and the observations. However, the standard model tended to over-predict GEM  
226 concentrations by about 10% across all sites (Table SI-1), with the greatest difference in the summer at DRI (+32%).

227 Modeled RM concentrations also varied by about a factor of 7 between sites (similar variance seen in the  
228 observations), with the highest concentrations predicted for MBO and SPL in the spring and summer, and the lowest  
229 predicted for LABS in the summer (Figure 1, Table SI-1). However, in terms of absolute difference in RM concentrations,  
230 the model over-predicted the observations by a factor of 2.5 overall.

231 The linear relationships between RM and other measured species (GEM,  $\text{O}_3$ , and WV) were determined both for  
232 the observations and the standard model. The slopes between observed RM vs. GEM daily concentrations were  
233 negative at all sites during the summer, and the standard model reproduced this RM/GEM trend at all sites (except for  
234 LABS) (Figure 2, Figure 3, and Table SI-2). Positive slopes were observed between observed RM and  $\text{O}_3$  at all sites  
235 (significant at MBO, NV02, and SPL) during the summer, and this trend was duplicated by the standard model (significant  
236 at all sites). Negative slopes between RM and WV were also observed (significant at all sites except SPL) and modeled  
237 (significant at all sites) for data from the summer. Negative correlations of RM with GEM and WV and positive  
238 correlations of RM with  $\text{O}_3$  both in the observations and the standard model are consistent with RM being formed in the  
239 free troposphere (where WV was low and  $\text{O}_3$  was high) from the photo-oxidation of GEM (resulting in low GEM).

240 In contrast to the summer time period, however, there was a greater lack of agreement between the model and  
241 observations for the spring data in Figure 2 and Table SI-2. The slopes of interspecies correlations of observed RM with  
242 GEM were about a factor of 2 less negative during the spring compared to the summer at MBO and SPL (Figure 2). At  
243 LABS, the spring RM/GEM ratio was a factor of 4 less negative compared to the summertime ratio, and at DRI the  
244 RM/GEM ratio was positive (Figure 2). Modeled RM/GEM ratios did not show the same seasonal trend, but instead  
245 were similar across spring and summer ( $\sim -275$  for MBO,  $\sim -150$  for DRI and  $\sim -350 \text{ pg ng}^{-1}$  for SPL). For RM: $\text{O}_3$  the  
246 observed ratios were positive and the observed RM:WV ratios were negative at all sites during the summer, but during  
247 the spring, these ratios did not show a consistent pattern (Figure 2).

248 Slopes of GOM vs. GEM of around -1 have been reported previously (Swartzendruber et al., 2006; Lyman and  
249 Jaffe, 2012). These have been for specific events, when one particular air mass has been measured, and when total  
250 gaseous Hg is likely constant. For these conditions, a slope of -1 indicates that photochemical conversion of GEM to  
251 GOM has occurred and there have been limited losses of GOM due to scavenging and deposition, and limited  
252 replenishment of GEM from the background pool. The RM/GEM slopes reported in Figure 2 and Table SI-2 are greater  
253 than -1 (or  $-1000 \text{ pg ng}^{-1}$ ), in other words, the slopes are less steep and the relationship between RM and GEM is weaker  
254 than the ideal -1 slope. For these data we do not expect a slope of -1 since these are across an entire season. Over such



255 a long time period, GEM concentrations do not stay constant, especially at DRI which has regular inputs from local  
256 natural enrichment, scavenging occurs at varying rates, and thus the lifetime of RM is highly variable.

### 259 *3.3 Case Study of Free Tropospheric Transport*

260 This study also compared observed and modeled data on 12-hr time resolution during a period of subsiding air  
261 across western North America (see weather maps and back trajectories shown in Supplemental Information) when  
262 observed RM concentrations were elevated. This event occurred during the week of June 20-25, 2007, when 12-hr  
263 maximum concentrations of the RM reached 260, 250, and 100  $\text{pg m}^{-3}$  at MBO, DRI, and NV02, respectively (Figure 4 a, f,  
264 i). These maximum values were observed at the 3 sites sequentially in time along a west-east transect from central  
265 Oregon to northern Nevada. Maximum RM concentrations occurred at MBO during the night when downslope flow was  
266 observed, and maximum RM concentrations at DR and NV02 occurred during the day when convective mixing was at its  
267 maximum.

268 Observed 12-hour mean GEM concentrations associated with the RM maxima were 1.0, 1.2, and 1.0  $\text{ng m}^{-3}$  at  
269 MBO, DRI, and NV02, respectively (Figure 4 b, e, h), all significantly lower than the seasonal means of GEM at each site.  
270 The diurnal pattern in GEM can be seen in Figure 4e and 4h for DRI and NV02, with higher concentrations during the  
271 night (12 UTC) and lower concentrations during the day (0 UTC) due to accumulation in the boundary layer and local  
272 geologic emission of GEM.

273 MBO experienced the highest 3-hour RM concentration of the three sites at 547  $\text{pg m}^{-3}$ , however, as discussed  
274 by Timonen et al. (2013) this event was meteorologically complex. High RM was first observed in an unusually low  $\text{O}_3$   
275 air mass (23 ppb) but then  $\text{O}_3$  recovered to more typical values (Figure 4a), while RM remained high (Figure 4c) and water  
276 vapor was relatively low throughout this period (Figure 4a). We interpret the RM event as follows: June 21 brought an  
277 air mass to MBO that was transported at low latitudes and was photochemically processed, with a maximum CO  
278 concentration of only 63 ppb, maximum particle scattering of  $1 \text{ Mm}^{-1}$ , and the aforementioned  $\text{O}_3$  concentration, and  
279 labeled as a “marine boundary layer” event by Timonen et al. 2013. This event was followed by another RM event on  
280 June 22, when  $\text{O}_3$  rebounded to 50 ppb which is more characteristic of FT air (Figure 4a). Further evidence of the  
281 transport is given by the gridded frequency distribution of HYSPLIT back trajectories shown in the supporting  
282 information (Figure SI-3). At MBO, modeled  $\text{O}_3$  and WV concentrations during June 20-26 were higher and lower,  
283 respectively than the observations, whereas at DRI and NV02 the model-observation agreement was better. We suspect  
284 that the global model did not reproduce the observed  $\text{O}_3$  concentrations at MBO due to the complex transport that was  
285 evident from the back trajectories.

286 Observed water vapor concentrations at DRI and NV02 (Figure 4 d, g) were equivalent to, or lower than WV  
287 observed at MBO (Figure 4a), corresponding to minimum relative humidity values of 17%, 6%, and 3%, at MBO, DRI, and

288 NV02 respectively. This indicates the very dry conditions in the desert and may have contributed to the longer lifetime  
289 of RM in the atmosphere and also perhaps the better collection efficiency of the analytical system.

290 The RM/GEM mean ratio calculated using the data including the maximum and minimum concentrations during  
291 the events followed both a longitudinal and elevation trend. At the western-most and highest elevation site, MBO, the  
292 RM/GEM event ratio was  $-1020 \pm 209 \text{ pg ng}^{-1}$ , compared with  $-568 \pm 60 \text{ pg ng}^{-1}$  at DRI and  $-173 \pm 33 \text{ pg ng}^{-1}$  at NV02,  
293 which was the eastern-most and lowest elevation site. The nearness of the RM/GEM ratio to -1000 at MBO suggests  
294 approximate “mass conservation” between RM and GEM. Slopes of less than -1000 can indicate some combination of  
295 loss of RM due to deposition, air mass mixing with varying total Hg concentrations, and varying air chemistries producing  
296 different forms of RM that have different collection efficiencies by the KCl-denuder (Huang et al., 2013).

297 Model output from two simulations is also shown for this time: the standard Hg-model with Br-oxidation and  
298 the OH-O<sub>3</sub> model with the oxidation scheme involving OH and O<sub>3</sub> (Figure 4 b, c, e, f, h, i). At MBO the model simulation  
299 with the OH-O<sub>3</sub> chemistry provided a closer match in timing of peak RM concentrations (within 12-hours) compared to  
300 the Br simulation (RM peak was 2-days later) (Figure 4c). The simulated RM/GEM slopes for the MBO event were  $-850$   
301  $\text{pg ng}^{-1}$  and  $-750 \text{ pg ng}^{-1}$  for the Br and OH-O<sub>3</sub> simulations, respectively. Both model runs matched the timing of the RM  
302 peak at DRI within 12-hours (Figure 4f) and NV02 within 24-hours (Figure 4i).

### 304 3.4 Testing Model Oxidation

305 RM and GEM observations were compared with Hg model simulations using two different oxidation schemes: Br  
306 and OH-O<sub>3</sub>, the reactions of which are listed above (cf. Holmes et al. (2010) and Selin et al. (2008), respectively). Bromine  
307 reaction kinetics are more widely accepted than the OH-O<sub>3</sub> kinetic pathway, but there are still large uncertainties and  
308 present instruments cannot directly confirm the chemical composition of RM, and therefore, the oxidation mechanisms  
309 in the atmosphere are not known. Thus, we ran GEOS-Chem with either the OH-O<sub>3</sub> or the Br kinetics and compared with  
310 the observations to test whether there was evidence for different oxidants of GEM or a single global oxidant. Daily  
311 mean RM and GEM concentrations from the observations at MBO and DRI and the two model runs are shown in Figure  
312 5. Note that the standard and OH-O<sub>3</sub> models provide similar RM concentrations but different GEM concentrations.

313 Correlations across the time series in Figure 5 between observations and each model run for RM and GEM for  
314 MBO and DRI, are shown in Figure 6. For GEM at both sites but more so at DRI, the OH-O<sub>3</sub> model more closely matched  
315 the observations (steeper slope) compared to the Br model, (Figure 6). For RM the OH-O<sub>3</sub> model also produced steeper  
316 slopes and larger  $r^2$  values compared to the Br model, again most notably at DRI. Simulated RM concentrations from the  
317 Br model were notably smaller than the observations during the summer at DRI. This is significant because RM is  
318 probably already a lower bound on real ambient concentrations due to inefficiencies associated with the collection  
319 method.

320 Figure 7 shows monthly mean RM/GEM ratios in the observations plotted against monthly mean RM/GEM ratios  
321 in the model using the Br-oxidation scheme (left panel) and the OH-O<sub>3</sub> oxidation scheme (right panel). Both the

322 observations and the model agree that the higher RM/GEM ratios occurred in the summer months, and lower RM/GEM  
323 ratios occurred in the spring. This is consistent with greater photochemical conversion of GEM and greater loss via dry  
324 deposition during the spring (Sigler et al., 2009). Modeled RM/GEM using either oxidation scheme was on average  $2.5 \pm$   
325  $2.6$  higher than the mean observed RM/GEM, a factor roughly in line with the estimate of collection inefficiency of the  
326 KCl-denuder (Gustin et al., 2013).

327 Note that in Figure 7 the RM/GEM ratios using the Br-oxidation scheme fall into two patterns: data with a higher  
328 slope which include those from DRI and NV02 (the desert sites), and data with a lower slope which include those from  
329 MBO and SPL (the mountain top sites). In contrast, the RM/GEM ratios using the OH-O<sub>3</sub>-oxidation scheme from all sites  
330 generally fall along one line. This is a consequence of higher RM concentrations and lower GEM concentrations modeled  
331 using the OH-O<sub>3</sub> oxidation scheme relative to the Br-scheme, as shown in Figure 5. The increase in RM concentrations  
332 modeled with the OH-O<sub>3</sub> scheme relative to the Br-scheme is greater for the desert sites than for MBO and SPL, the  
333 mountain top sites. This result suggests the presence of different chemical regimes in different parts of the troposphere  
334 and signals that there is not necessarily one single global oxidant. Future GEOS-Chem work should investigate the effect  
335 of Br- and O<sub>3</sub>- initiated gas-phase oxidation occurring simultaneously in the atmosphere, as well as aqueous and  
336 heterogeneous reactions.

#### 337 **4.0 Conclusions**

338 In this study, we have compiled the available speciated atmospheric Hg measurements from three high  
339 elevation and two mid-elevation sites (4 in the U.S. and 1 in Taiwan) and compared to the GEOS-Chem global Hg model  
340 with two different oxidation schemes in order to examine spatio-temporal trends both in the observations and the  
341 model and to test for evidence of multiple GEM oxidation pathways in the atmosphere. Overall, the comparison  
342 between observed mercury species (GEM and RM) and those from the standard model showed a relatively weak  
343 relationship, which demonstrates the need to strengthen our understanding of fundamental chemistry and  
344 measurement artifacts. Where the observations and the standard model agreed was in displaying negative correlations  
345 between RM and GEM, negative correlations between RM and WV, and positive correlations between RM and O<sub>3</sub>. This  
346 indicated the tendency of RM to be produced in dry upper altitude air from the photo-oxidation of GEM. A case study of  
347 a wide scale subsidence event observed from Oregon to Nevada at 3 sites sequentially, showed that RM concentrations  
348 were enhanced and GEM concentrations were depleted, with an observed RM/GEM ratio at MBO of  $-1020 \pm 209 \text{ pg ng}^{-1}$ ,  
349 a slope suggesting stoichiometric conversion of Hg<sup>0</sup> to Hg<sup>II</sup> and minimal analytical collection inefficiencies. The  
350 correlations in the observations were weaker in the spring compared to the summer but not in the standard model  
351 suggesting a seasonal change in the sources and/or sinks of RM that was not simulated in the model and/or a seasonal  
352 change in the collection efficiency of the method. The variability of seasonal mean observed RM concentrations across  
353 sites was about a factor of 7 with the highest concentrations seen at DRI and at MBO in the summer and the lowest at  
354 LABS in the summer. The standard model also simulated mean RM concentrations that varied by about a factor of 7  
355 across sites, but these concentrations were offset positively from the observations by a mean factor of 2.5 across all

356 sites. However, the model offset was not equivalent at all sites, with mean observed RM concentrations across 3  
357 consecutive summers at DRI being slightly higher than RM concentrations from the standard model (76 vs. 72  $\mu\text{g m}^{-3}$ ).  
358 When the model was run with the OH-O<sub>3</sub> oxidation scheme instead of the Br oxidation scheme, it was found that mean  
359 concentrations of RM were higher and GEM were lower, especially at the desert sites DRI and NV02, producing better  
360 correlations between measured/modeled RM and GEM compared to the model with the Br-oxidation scheme. This is  
361 consistent with multiple GEM oxidation pathways occurring in the atmosphere and hence multiple forms of RM.

## 362 Acknowledgements

363 The authors wish to thank SPL personnel Gannet Hallar, Ian McCubbin, and Xavier Faïn, and the Taiwan  
364 Environmental Protection Administration for financially supporting the atmospheric Hg monitoring at LABS. We would  
365 also like to thank the past UNR graduate students that collected the DRI and NV02 data, Seth Lyman and Christiana  
366 Peterson, and Harvard graduate student Hannah Horowitz. We also thank the anonymous reviewers for their useful  
367 comments.

## 370 References

- 371 Ambrose, J.L., Reidmiller, D.R., Jaffe, D.A., 2011. Causes of high O<sub>3</sub> in the lower free troposphere over the Pacific  
372 Northwest as observed at the Mt. Bachelor Observatory. *Atmos. Environ.* 45, 5302–5315.
- 373 Ambrose, J. L., Lyman, S. N., Huang, J. Gustin, M. S., Jaffe, D. A., 2013. Fast Time Resolution Oxidized Mercury  
374 Measurements during the Reno Atmospheric Mercury Intercomparison Experiment (RAMIX), *Environmental Science &*  
375 *Technology*, 47 (13), 7285-7294.
- 376 Amos, H.M., Jacob, D.J., Holmes, C.D., Fisher, J.A., Wang, Q., Yantosca, R.M., Corbitt, E.S., Galarneau, E., Rutter, A.P.,  
377 Gustin, M.S., Steffen, A., Schauer, J.J., Graydon, J.A., St. Louis, V.L., Talbot, R.W., Edgerton, E.S., Zhang, Y., and  
378 Sunderland, E.M., 2012. Gas-particle partitioning of atmospheric Hg(II) and its effect on global mercury deposition,  
379 *Atmos. Chem. Phys.* 12, 591–603.
- 380 Bolton, D., 1980. The computation of equivalent potential temperature. *Monthly Weather Review* 108, 1046-1053.
- 381 Castro MS, Moore C, Sherwell J, Brooks SB. Dry deposition of gaseous oxidized mercury in Western Maryland. *Sci Total*  
382 *Environ* 2012;417:232–40.
- 383 Dibble, T. S, Zelic, M. J., Mao, H. Thermodynamics of reactions of ClHg and BrHg radicals with atmospherically abundant  
384 free radicals *ATMOSPHERIC CHEMISTRY AND PHYSICS* Volume: 13 Issue: 18 Pages: 9211-9212 DOI: 10.5194/acp-13-  
385 9211-2013
- 386 Faïn, X., Obrist, D., Hallar, A.G., McCubbin, I., Rahn, T., 2009. High levels of reactive gaseous mercury observed at a high  
387 elevation research laboratory in the Rocky Mountains. *Atmos. Chem. Phys.* 9, 8049–8060, doi:10.5194/acp-9-8049-2009.
- 388 Goodsite, M., Plane, J., and Skov, H.: A theoretical study of the oxidation of Hg<sup>0</sup> to HgBr<sub>2</sub> in the troposphere, *Environ. Sci.*  
389 *Technol.*, 38, 1772–1776, doi:10.1021/es034680s, 2004.
- 390 Gustin, M.S., Jaffe, D.A., 2010. Reducing the uncertainty in measurement and understanding of mercury in the  
391 atmosphere. *Environ. Sci. Technol.* 44, 2222–2227.

392 Gustin, M.S. 2011. Exchange of Mercury between the Atmosphere and Terrestrial Ecosystems. In: Liu G, Cai Y, O’driscoll  
393 N, editors. Chapter 13 in *Environmental Chemistry and Toxicology of Mercury*. John Wiley and Sons, p. 423–52.

394 Gustin, M.S., Weiss-Penzias, P. Peterson, C., 2012. Investigating sources of gaseous oxidized mercury in dry deposition  
395 at three sites across Florida, USA. *Atmos. Chem. Phys.* 12, 9201–9219.

396 Gustin, M.S., Huang, J., Miller, M.B., Finley, B.D., Call, K., Ambrose, J.L., Peterson, C., Lyman, S.N., Everhart, S., Bauer, D.,  
397 Remeika, J., Hynes, A., Jaffe, D.A., Lindberg, S.E. 2013. RAMIX – a step towards understanding mercury atmospheric  
398 chemistry and Tekran® observations, *Environ. Sci. Technol.*, 47 (13), pp 7295–7306.

399 Hall, B., 1995. The gas phase oxidation of elemental mercury by ozone, *Water Air Soil Poll.* 80, 301–315.

400 Holmes, C., Jacob, D., Yang, X., 2006. Global lifetime of elemental mercury against oxidation by atomic bromine in the  
401 free troposphere. *Geophys. Res. Lett.* 33, L20808, doi:10.1029/2006GL027176.

402 Holmes, C.D., Jacob, D.J., Corbitt, E.S., Mao, J., Yang, X., Talbot R., Slemr, F., 2010. Global atmospheric model for mercury  
403 including oxidation by bromine atoms. *Atmos. Chem. Phys.* 10, 12037–12057, doi:10.5194/acp-10-12037-2010.

404 Huang JY, Gustin MS. Evidence for a Free Troposphere Source of Mercury in Wet Deposition in the Western United  
405 States. *Environmental Science & Technology* 2012; 46: 6621-6629.

406 Huang, J.Y., Miller, M.B., Weiss-Penzias, P., Gustin, M.S., Comparison of reactive mercury measurements made with KCl-  
407 coated denuders, nylon membranes, and cation exchange membranes, submitted to *Environmental Science and*  
408 *Technology*, 2013.

409 Hynes, A. J.; Donohoue, D. L.; Goodsite, M. E.; Hedgecock, I. M. Our Current Understanding of Major Chemical and  
410 Physical Processes Affecting Mercury Dynamics in the Atmosphere and at the Air-Water/Terrestrial Interfaces. In  
411 *Mercury Fate and Transport in the Global Atmosphere*; Mason, R., Pirrone, N., Eds.; Springer: New York, 2009.

412 Jaffe, D., Prestbo, E., Swartzendruber, P., Weiss-Penzias, P., Kato, S., Takami, A., Hatakeyama, S., Kajii, Y., 2005. Export of  
413 atmospheric mercury from Asia. *Atmos. Environ.* 39, 3029– 3038.

414 Jaffe, D., S. Lyman, H. Amos, M. Gustin, J. Huang, N. Selin, L. Levin, A. Ter Schure, R. Mason, R. Talbot, A. Rutter, B. Finley,  
415 L. Jaeglé, V. Shah, C. McClure, J. Ambrose, L. Gratz, S. Lindberg, P. Weiss-Penzias, G-R. Sheu, D. Feddersen, M. Horvat, A.  
416 Dastoor, A. Hynes, H. Mao, J. Sonke, F. Slemr, J. Fisher, R. Ebinghaus, Y. Zhang, G. Edwards, 2014. Progress on  
417 understanding atmospheric mercury hampered by uncertain measurements, *Environmental Science and Technology*,  
418 Accepted.

419 Kos, G. Ryzhkov, A. Dastoor, A. Narayan, J. Steffen, A. Ariya, P. A. Zhang, L., 2013. Evaluation of discrepancy between  
420 measured and modelled oxidized mercury species. *Atmos. Chem. Phys.*, 13, 4839–4863; DOI 10.5194/acp-13-4839-2013.

421 Landis, M.S., Stevens, R.K., Schaedlich, F., and Prestbo, E.M., 2002. Development and characterization of an annular  
422 denuder methodology for the measurement of divalent inorganic reactive gaseous mercury in ambient air. *Environ. Sci.*  
423 *Technol.* 36, 3000–3009.

424 Lindberg, S.E., Stratton, W.J., 1998. Atmospheric mercury speciation: concentrations and behavior of reactive gaseous  
425 mercury in ambient air. *Environ. Sci. Technol.* 32, 49–57.

426 Lyman, S.N., Gustin, M.S., 2008. Speciation of atmospheric mercury at two sites in northern Nevada, USA. *Atmos.*  
427 *Environ.* 42, 927– 939, doi:10.1016/j.atmosenv.2007.10.012.

428 Lyman, S.N., Jaffe, D.A., Gustin, M.S., 2010. Release of mercury halides from KCl denuders in the presence of ozone.  
429 *Atmos. Chem. Phys.* 10, 8197–8204, doi:10.5194/acp-10-8197-2010.

430 Lyman, S.N., Jaffe, D.A., 2011. Formation and fate of oxidized mercury in the upper troposphere and lower stratosphere.  
431 *Nat. Geosci.* 5, 114–117, doi:10.1038/NGEO1353.

432 McClure, C. D., Jaffe, D. A., Edgerton, E.S.: Evaluation of the KCl Denuder Method for Gaseous Oxidized Mercury using  
433  $\text{HgBr}^2$  at an In-Service AMNet Site, *Environ. Sci. Technol.*, 48 (19), 11437-11444, 2014.

434 Moore, C.W., Obrist, D., Luria, M., 2013. Atmospheric mercury depletion events at the Dead Sea: Spatial and temporal  
435 aspects. *Atmospheric Environment*, 69, 231-239.

436 Moore, C.W., Obrist, D., Steffen, A., Staebler, R., Douglas, T., Richter, A., Nghiem, S., 2014. Convective forcing of mercury  
437 and ozone in the Arctic boundary layer induced by leads in sea ice. *Nature*, 506, doi:10.1038/nature12924.

438 Murphy, D.M., Hudson P.K., Thompson, D.S., Sheridan, P.J., Wilson, J.C., 2006. Observations of mercury-containing  
439 aerosols. *Environ. Sci. Technol.* 40, 3163–3167.

440 Obrist, D., Hallar, A.G., McCubbin, I., Stephens, B.B., Rahn, T., 2008. Atmospheric mercury concentrations at Storm Peak  
441 Laboratory in the Rocky Mountains: Evidence for long-range transport from Asia, boundary layer contributions, and  
442 plant mercury uptake. *Atmos. Environ.* 42, 7579–7589, doi:10.1016/j.atmosenv.2008.06.051.

443 Pacyna, E.G., Pacyna, J.M., Sundseth, K., Munthe, J., Kindbom, K., Wilson, S., Steenhuisen, F., Maxson, P., 2010. Global  
444 emission of mercury to the atmosphere from anthropogenic sources in 2005 and projections to 2020. *Atmos. Environ.*  
445 44, 2487–2499, doi:10.1016/j.atmosenv.2009.06.009.

446 Peterson, C., Gustin, M., Lyman, S., 2009. Atmospheric mercury concentrations and speciation measured from 2004 to  
447 2007 in Reno, Nevada, USA. *Atmos. Environ.* 43, 4646–4654.

448 Pirrone, N., Cinnirella, S., Feng, X., Finkelman, R.B., Friedli, H.R., Leaner, J., Mason, R., Mukherjee, A.B., Stracher, G.B.,  
449 Streets, D.G., Telmer, K., 2010. Global mercury emissions to the atmosphere from anthropogenic and natural sources.  
450 *Atmos. Chem. Phys.* 10, 5951–5964.

451 Sather ME, Mukerjee S, Smith L, Mathew J, Jackson C, Callison R, et al. Gaseous oxidized mercury dry deposition  
452 measurements in the Four Corners Area and Eastern Oklahoma, *U.S.A Atmos Pollut Res* 2013;4(2):168–80.

453 Schroeder, W.H., Munthe, J., 1998. Atmospheric mercury – An overview. *Atmos. Environ.* 32, 809–822.

454 Selin, N. E. and Jacob, D. J.: Seasonal and spatial patterns of mercury wet deposition in the United States: Constraints on  
455 the contribution from North American anthropogenic sources, *Atmos. Environ.*, 42, 5193–5204,  
456 doi:10.1016/j.atmosenv.2008.02.069, 2008.

457

458 Selin, N. E., Jacob, D. J., Yantosca, R. M., Strode, S., Jaegl' e, L., and Sunderland, E. M.: Global 3-D land-ocean-atmosphere  
459 model for mercury: Present-day versus preindustrial cycles and anthropogenic enrichment factors for deposition, *Global*  
460 *Biogeochem. Cyc.*, 22, 1–13, doi:10.1029/2007GB003040, 2008.

461 Sheu, G.-R., Lin, N.-H., Wang, J.-L., Lee, C.-T., Ou Yang, C.-F., Wang, S.-H., 2010. Temporal distribution and potential  
462 sources of atmospheric mercury measured at a high-elevation background station in Taiwan. *Atmos. Environ.* 44,  
463 2393–2400.

464 Sheu, G.-R., Lin, N.-H., Lee, C.-T. Wang, J.-L., Chuang, M.-T., Wang, S.-H., Chi, K.H., Ou Yang, C.-F., 2012. Distribution of  
465 atmospheric mercury in northern Southeast Asia and South China Sea during Dongsha Experiment. *Atmos. Environ.*,  
466 doi/10.1016/j.atmosenv.2012.07.002.

467 Sigler, J. M., Mao, H., and Talbot, R.: Gaseous elemental and reactive mercury in Southern New Hampshire, *Atmos.*  
468 *Chem. Phys.*, 9, 1929–1942, doi:10.5194/acp-9-1929-2009, 2009.

469 Slemr, F., Angot, H., Dommergue, A., Magand, O., Barret, M., Weigelt, A., Ebinghaus, R., Brunke, E.-G., Pfaffhuber, K.,  
470 Edwards, G., Howard, D., Powell, J., Keywood, M., Wang, F., 2014. Comparison of mercury concentrations measured at  
471 several sites in the Southern Hemisphere, *Atmos. Chem. Phys. Discuss.*, 14, 30611–30637.

472 Soerensen, A. L., Skov, H., Jacob, D. J., Soerensen, B. T., and Johnson, M. S.: Global concentrations of gaseous elemental  
473 mercury and reactive gaseous mercury in the marine boundary layer, *Environ. Sci. Technol.*, 44, 425–427, 2010.

474 Strode, S. A., L. Jaegle', D. A. Jaffe, P. C. Swartzendruber, N. E. Selin, C. Holmes, and R. M. Yantosca (2008), Trans-Pacific  
475 transport of mercury, *J. Geophys. Res.*, 113, D15305, doi:10.1029/2007JD009428.

476 SubirM, Ariya PA, Dastoor AP. A review of uncertainties in atmospheric modeling of mercury chemistry I. Uncertainties  
477 in existing kinetic parameters: fundamental limitations and the importance of heterogeneous chemistry. *Atmos Environ*  
478 2011;45(32):5664–76.

479 Swartzendruber, P.C., Jaffe, D.A., Prestbo, E.M., Weiss-Penzias, P., Selin, N.E., Park, R., Jacob, D.J., Strode, S., Jaegle', L.,  
480 2006. Observations of reactive gaseous mercury in the free troposphere at the Mount Bachelor Observatory. *J. Geophys.*  
481 *Res.*, 111, D24301, doi:10.1029/2006JD007415.

482 Swartzendruber, P.C., Chand, D., Jaffe, D.A., Smith, J., Reidmiller, D., Gratz, L., Keeler, J., Strode, S., Jaegle', L., Talbot, R.,  
483 2008. Vertical distribution of mercury, CO, ozone, and aerosol scattering in the Pacific Northwest during the spring 2006  
484 INTEX-B campaign, *J. Geophys. Res.*, 113, D10305, doi:10.1029/2007JD009579.

485 Talbot, R., Mao, H., Scheuer, E., Dibb, J., Avery, M., 2007. Total depletion of Hg0 in the upper troposphere-lower  
486 stratosphere, *Geophys. Res. Lett.* 34, L23804, doi:10.1029/2007GL031366.

487 Timonen, H., Ambrose, J. L., and Jaffe, D. A.: Oxidation of elemental Hg in anthropogenic and marine air masses, *Atmos.*  
488 *Chem. Phys.*, 13, 2827-2836, doi:10.5194/acp-13-2827-2013, 2013.

489 Valente, R.J., Shea, C., Humes, K.L., Tanner R.L., 2007. Atmospheric mercury in the Great Smoky Mountains compared to  
490 regional and global levels. *Atmos. Environ.* 41, 1861–1873.

491 Weiss-Penzias, P., Jaffe, D.A., Swartzendruber, P., Dennison, J.B., Chand, D., Hafner, W., Prestbo, E., 2006. Observations  
492 of Asian air pollution in the free troposphere at Mount Bachelor Observatory during the spring of 2004. *J. Geophys. Res.*  
493 111, D10304, doi:10.1029/2005JD006522.

494 Weiss-Penzias, P., Gustin, M.S., Lyman, S.N., 2009. Observations of speciated atmospheric mercury at three sites in  
495 Nevada: evidence for a free tropospheric source of reactive gaseous mercury. *J. Geophys. Res.* 114, D14302,  
496 doi:10.1029/2008JD011607.

497 Wright, G., Miller, M.B., Weiss-Penzias P, Gustin, M Investigation of mercury deposition and potential sources at six  
498 sites from the Pacific Coast to the Great Basin, USA, *Science of the Total Environment* 470-471C (2014), pp. 1099-1113  
499 DOI information: 10.1016/j.scitotenv.2013.10.071

500 Zhang, L., Blanchard P., Johnson, D., Dastoor, A., Ryzhkov, A., Lin, C.J., Vijayaraghavan, K., Gay, D., Holsen, T.M., Huang,  
501 J., Graydon, J.A., St. Louis, V.L., Castro, M.S., Miller, E.K., Marsik, F., Lu, J., Poissant, L., Pilote, M., Zhang, K.M., 2012.  
502 Assessment of modeled mercury dry deposition over the Great Lakes region. *Environ. Pollut.* 161, 272-283.  
503

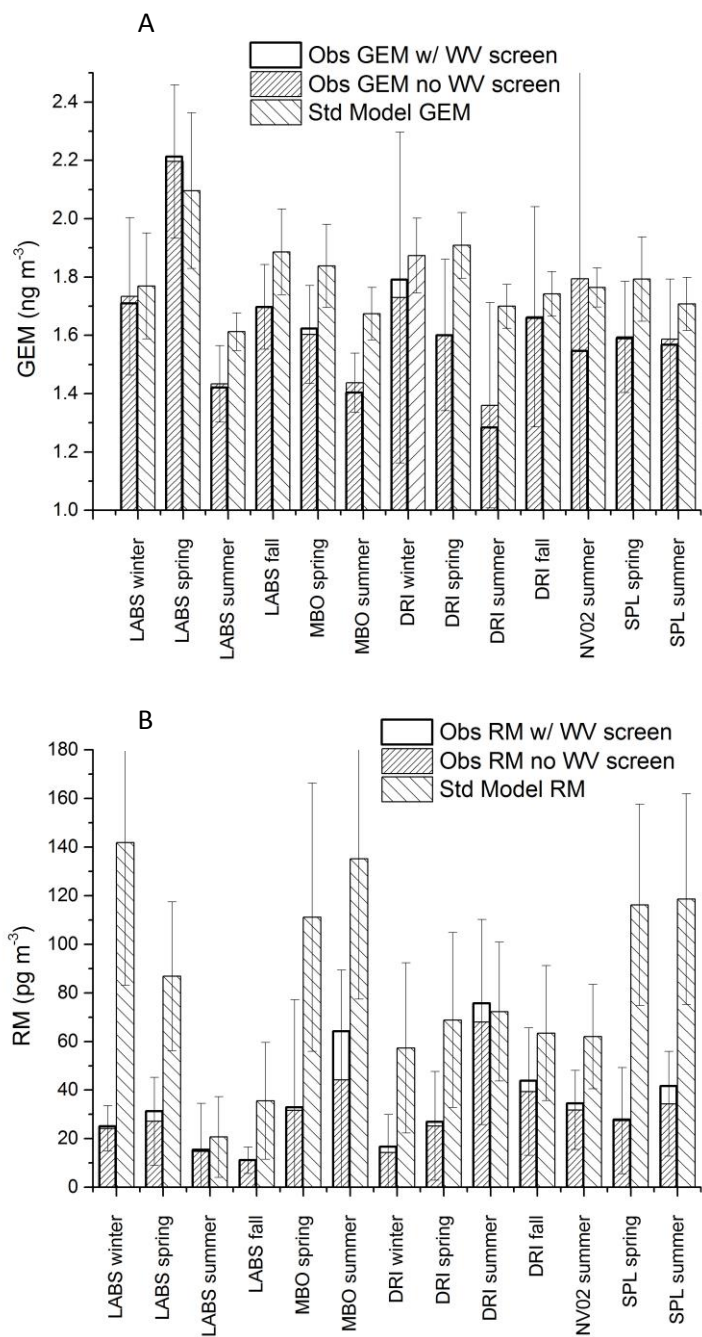
Table 1: Information on the five sites that are compared in this study<sup>1</sup> (listed from west to east).

Site	Site Abbrev.	Latitude	Longitude	Physical Setting	Elevation (m)	Periods of Measurement/Model Comparison
Mt. Front Lulin, Taiwan	LABS	23.51	120.92	Ridgetop summit, scrub forest	2862	2008: Mar 3-31, Jun 30-July 23, Aug 31-Sep 10, Nov 30-Dec 31
Mt. Bachelor, Oregon, USA	MBO	43.98	-121.69	Summit of dormant volcano, rock, ice	2763	2006: Apr 25-Jun 30 2007: Apr 17-Jul 17 2008: Mar 13-Jun 7 2009: May 1-20
Reno, Nevada, USA	DRI	39.57	-119.8	Foothills, 5 km N of Reno, desert scrub	1497	Jan 1, 2005 – Aug 21, 2007
Paradise Valley, Nevada, USA	NV02	41.5	-117.5	Valley within basin and range, sagebrush, cultivated alfalfa	1388	2007: Jun 13-Aug 21
Storm Peak, Colorado, USA	SPL	40.46	-106.74	Ridgetop summit, alpine	3200	2008: Apr 29-Jul 1

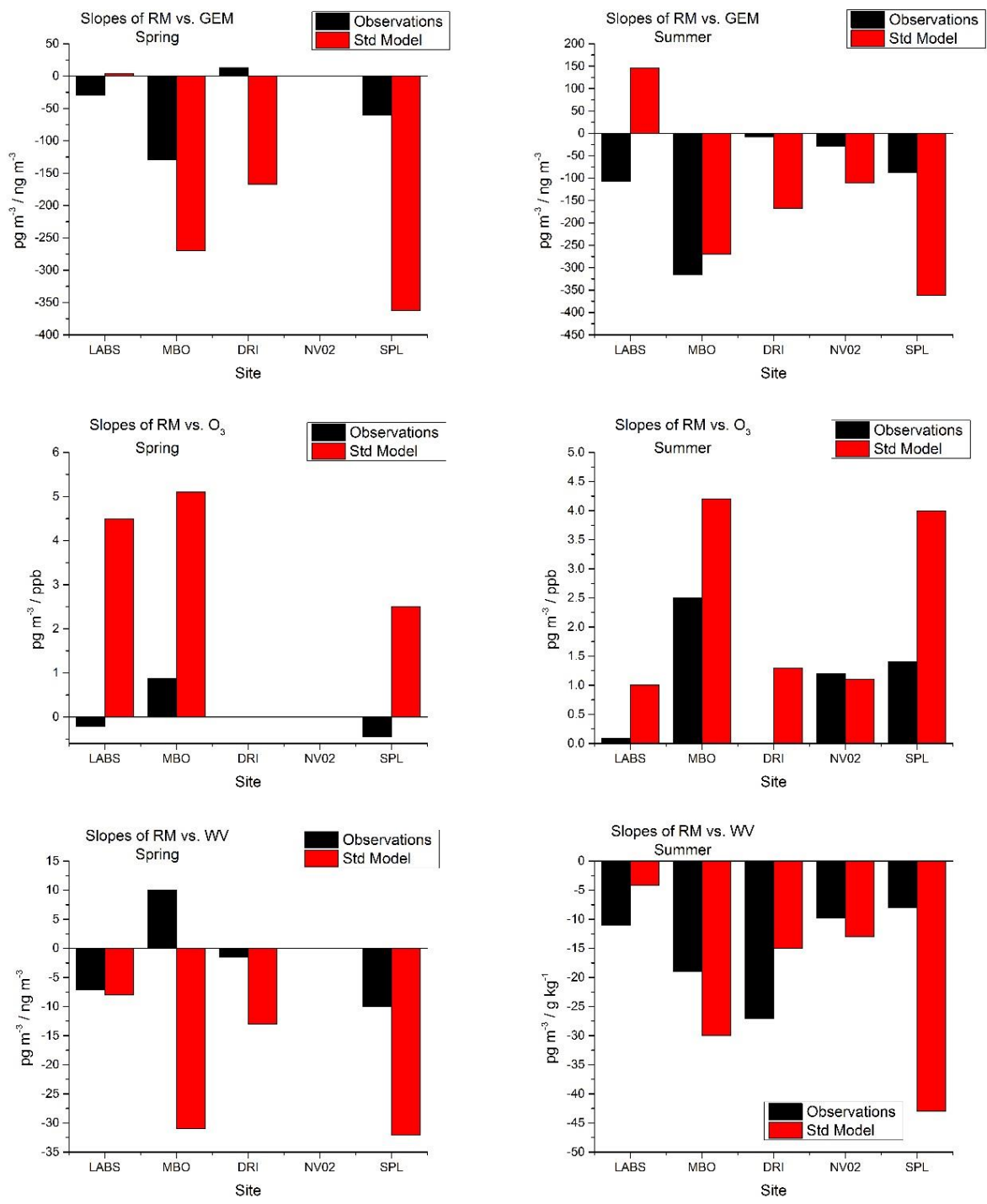
<sup>1</sup>Details of all these sites have been discussed elsewhere (Weiss-Penzias et al., 2006 (MBO), Fain et al., 2009 (SPL); Peterson et al., 2009 (DRI); Lyman and Gustin, 2008 (NV02); Sheu et al., 2010 (LABS))



505 Figure 1: Means and standard deviations of observed and standard-modeled (A) GEM and (B) RM for each site by  
 506 season. The WV screened data are plotted in the same column as the unscreened data.



511 Figure 2: Slopes from the linear regressions of observed and standard-modeled RM vs. GEM, RM vs. O<sub>3</sub>, and RM vs.  
 512 water vapor daily mean concentrations for each site and season. Observed data were filtered using only data when WV  
 513 < 75<sup>th</sup> percentile. Winter and fall data not shown. All linear regression statistics given in Table SI-2.



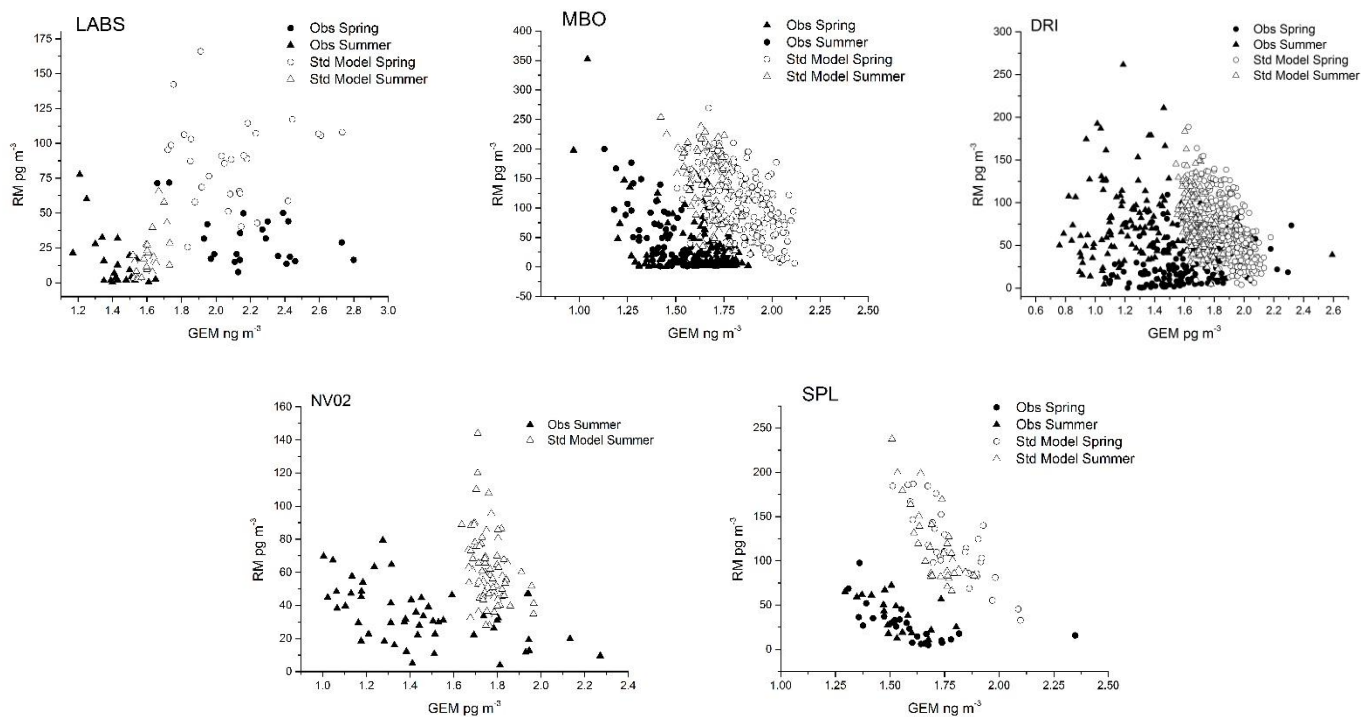
514

515

516

517

518 Figure 3: Scatter plots of RM vs. GEM daily mean concentrations for the WV-screened observations and the standard  
519 model delineated by site and season.



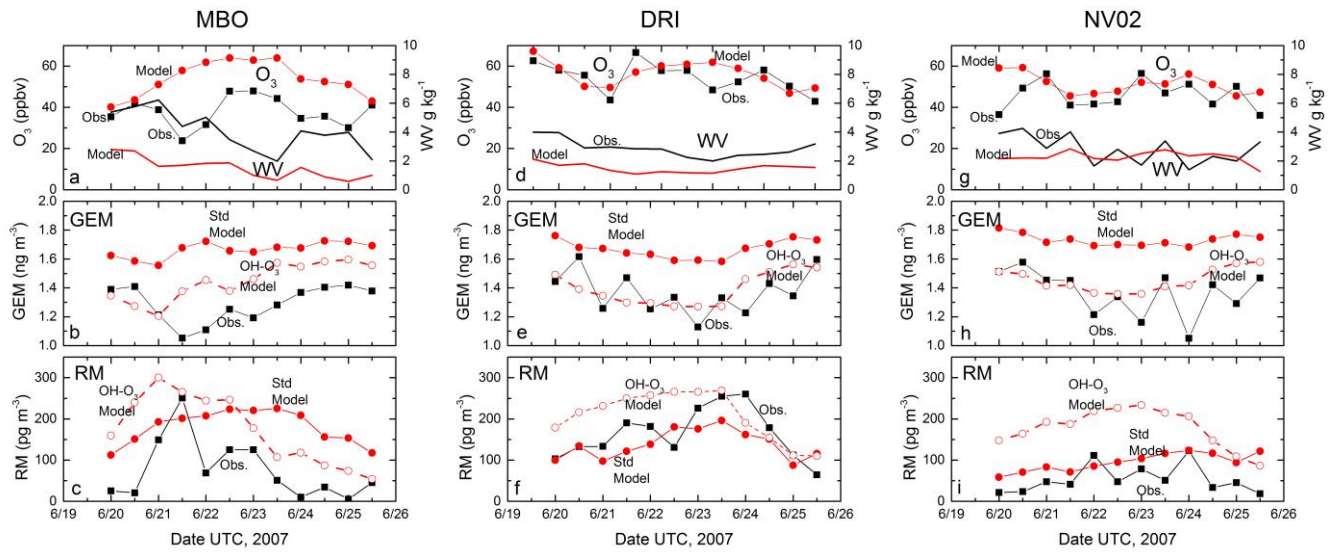
520

521

522

523  
524

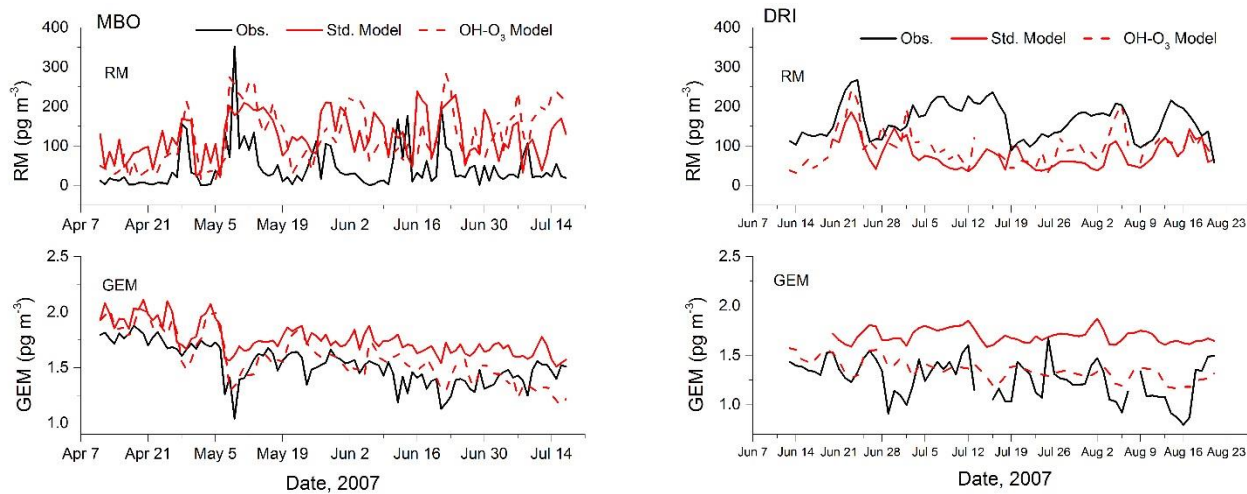
Figure 4 (a-i): Twelve-hour mean concentrations of O<sub>3</sub>, water vapor, GEM, and RM at three sites during a high-RM event during June 20-25, 2007. Observational, standard model, and OH-O<sub>3</sub> model data are shown.



525  
526

527 Figure 5: Comparison of observed, standard-modeled, and OH-O<sub>3</sub>-modeled RM and GEM daily mean concentrations for  
528 spring/summer 2007 at MBO and summer 2007 at DRI.

529

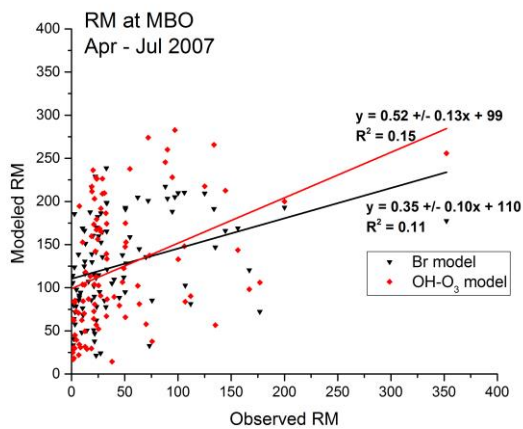
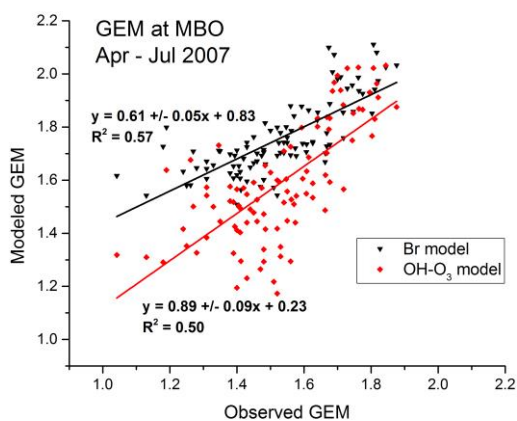


530

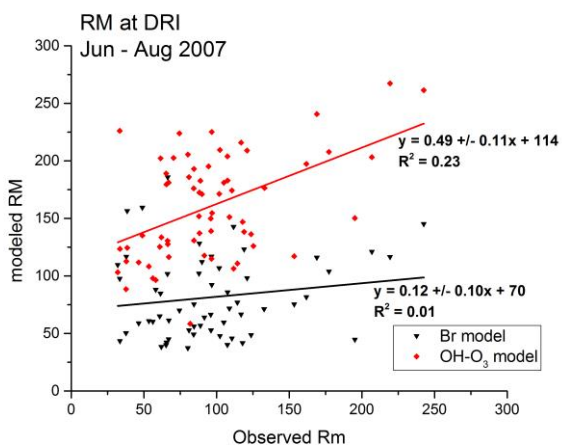
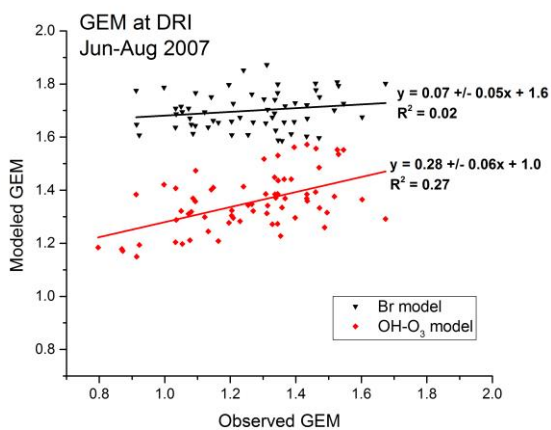
531

532

533 Figure 6: Comparison of linear relationships between GEM and RM in the observations with data from the model using  
534 either the Br or the OH-O<sub>3</sub> oxidation schemes.



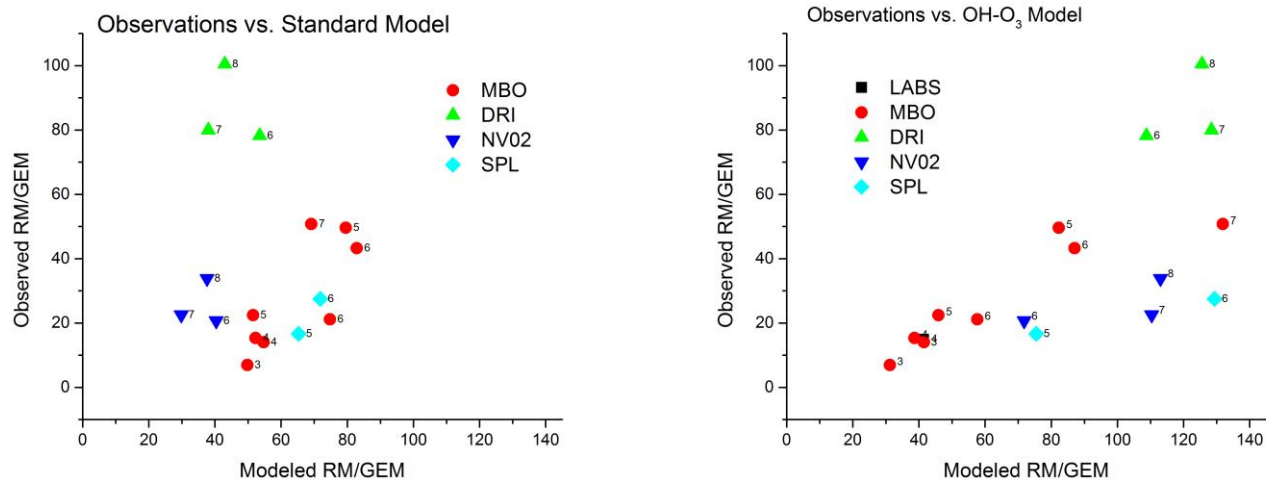
535



536

537

538 Figure 7: Plots of monthly mean RM/GEM from the observations vs. monthly mean RM/GEM in the standard model (left  
539 panel) and vs. monthly mean RM/GEM in the OH-O<sub>3</sub> model (right panel). The units are pg ng<sup>-1</sup>. The month is indicated  
540 by the labels on each data point. Only data from summer 2007 were considered for DRI since the model with OH-O<sub>3</sub>  
541 chemistry was not run for all time periods.



542

543

544